iScience

CellPress
OPEN ACCESS

Article

Color gamut characteristics of diffractive-light guides of near-eye augmented reality glasses

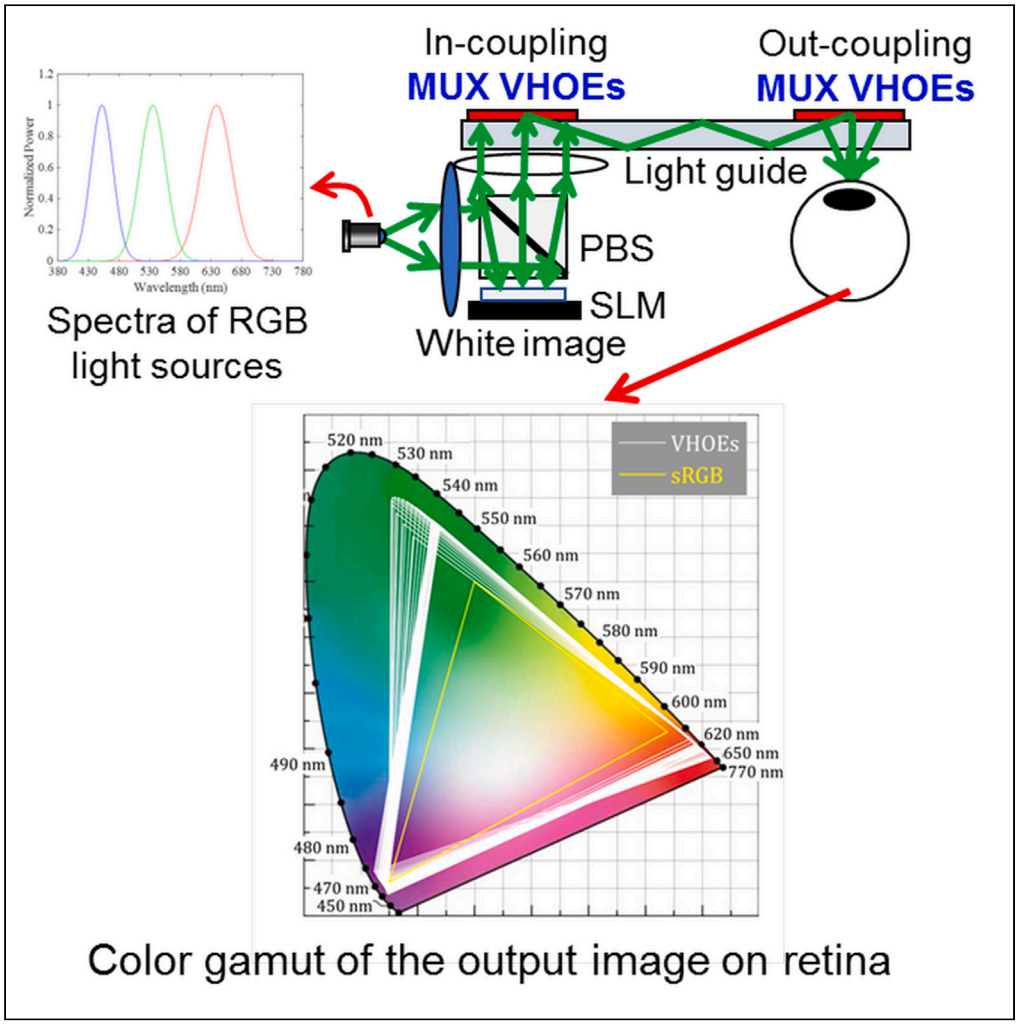

Ching-Cherng Sun, Wen-Kai Lin, Tsung-Hsun Yang, ..., Tsung-Xian Lee, Chih-Yuan Cheng, Shiuan Huei Lin

ccsun@dop.ncu.edu.tw (C.-C.S.)
lin@nycu.edu.tw (S.H.L.)

Highlights

Elucidate color gamut characteristics of diffractive light guides with SRG and VHOE

Novel approach employing holographic multiplexing can enhance common color gamut

The color gamut of VHOE-type light guide reach 130% sRGB, comparable with SRG-type

Sun et al., iScience 27, 110023
June 21, 2024
https://doi.org/10.1016/j.isci.2024.110023

iScience

CellPress
OPEN ACCESS

Article

Color gamut characteristics of diffractive-light guides of near-eye augmented reality glasses

Ching-Cherng Sun,[1,2,5,*] Wen-Kai Lin,[1] Tsung-Hsun Yang,[1] Zih-Fan Chen,[2] Chi Sun,[2] Wei-Chia Su,[3] Shao-Kui Zhou,[3] Yeh-Wei Yu,[1] Tsung-Xian Lee,[4] Chih-Yuan Cheng,[1] and Shiuan Huei Lin[2,5,6,*]

SUMMARY

We delve into the distinctive color gamut characteristics resulting from color dispersion of surface relief grating (SRG) and wavelength degeneracy of volume holographic optical element (VHOE) in a diffractive light guide. While a laser-like spectrum achieves an impressive 194% sRGB color gamut for both cases, it proves unsuitable for VHOE light guides due to limitations in breaking the field of view (FOV) of the display. Conversely, a broad-band light source, such as LEDs, offers continuous FOV but reduces the common color gamut to 50% sRGB. We then present a newly designed VHOE light guide capable of achieving the common color gamut of 130% sRGB using two multiplexed holograms of each color, closely matching the 133% sRGB achieved by an SRG light guide. This article presents the first theoretical methodology to elucidate color performance of diffractive light guides utilizing VHOEs with holographic multiplexing, affirming their suitability for crafting high-quality near-eye display.

INTRODUCTION

Large displays have become ubiquitous worldwide, thanks to the widespread adoption of liquid crystal technology, enabling expansive panels at a low cost. Despite this progress, a significant reduction in energy consumption can be achieved by ensuring that the display light is directed specifically toward the users' eyes. One potential solution lies in the development of near-eye glasses-type display designed to cater to individual users. The integration of mobile functionalities, such as augmented reality (AR) or even mixed reality (MR), could further enhance the capabilities of these glasses-type displays.[1] Both AR and MR glasses demand the seamless incorporation of virtual images into the user's surroundings with a see-through function.[1–6] Achieving this is feasible by embedding a beam-splitter in the glasses to efficiently couple incoming images from the top side. However, a critical consideration in the design of near-eye glasses-type display is the substantial impact on user comfort stemming from concerns about the device's volume and weight. To address this challenge, the incorporation of diffractive elements emerges as a viable solution. Figure 1 illustrates a conceptual diagram of a diffractive light guide for AR glasses. Diffractive optical elements (DOE) play a crucial role in directing incoming light into a specific direction, a functionality unattainable through optical elements based solely on reflection or refraction.[7] In the depicted figure, the couple-in DOE serves to diffract incoming light carrying an image to a direction within the scope of the propagation mode through total internal reflection (TIR) along the glass plate. Subsequently, the couple-out DOE redirects the guided light toward the user's eye.[8,9] In comparison with traditional approach with a beam splitter plate in the near-eye glasses,[10–12] this innovative use of diffractive elements not only addresses the energy efficiency concerns associated with display technologies but also contributes to a more streamlined and user-friendly design for near-eye glasses-type display.

Diffractive optical elements offer an effective means to optimize the volume of glasses and leverage the glass plate as a pivotal component. Currently, two distinct DOEs are employed in these glasses, differing primarily in thickness, and the key distinction lies in the presence of the Bragg condition. The first category encompasses thin gratings, with the surface relief grating (SRG) serving as a representative element. The diffraction from a thin grating arises from constructive interference along the lateral plane of the grating, which lacks effective thickness, such that it has the capability to diffract incoming white light into a split light exhibiting a rainbow-like structure, as illustrated in Figure 2A. SRGs can be manufactured through a lithography process to create a surface structure, providing a distinct advantage in terms of mass production efficiency.[13–18]

The second group comprises volume gratings and holograms, where thickness becomes a critical factor in influencing diffraction.[19–23] The diffraction from volume grating relies on constructive interference across the entire volume, leading to the imposition of the Bragg condition,

[1]Department of Optics and Photonics, National Central University, Chung-Li 320317, Taiwan
[2]Department of Electrophysics, National Yang Ming Chiao Tung University, HsinChu 30010, Taiwan
[3]Graduate Institute of Photonics, National Changhua University of Education, Changhua 50074, Taiwan
[4]Graduate Institute of Color and Illumination Technology, National Taiwan University of Science and Technology, Taipei 10607, Taiwan
[5]These authors contributed equally
[6]Lead contact
*Correspondence: ccsun@dop.ncu.edu.tw (C.-C.S.), lin@nycu.edu.tw (S.H.L.)
https://doi.org/10.1016/j.isci.2024.110023

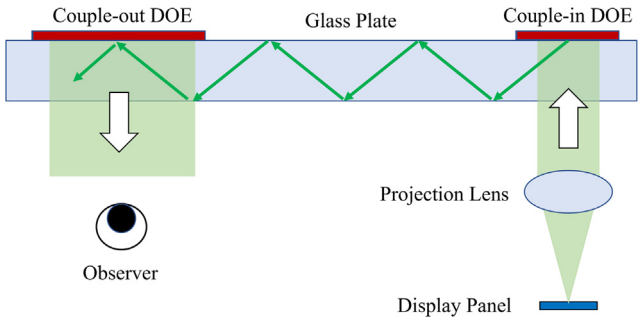

Figure 1. A schematic diagram of a diffractive light guide system
Here the image from the display panel is projected to the light guide, and the DOEs play roles of couple in and couple out function through the glass plate.

which restricts diffraction along a specific direction with a designated wavelength.[24–26] Consequently, a volume grating can diffract incoming light into a split light with a rainbow-like structure, where each wavelength of the diffracted light corresponds to a specific incident angle determined by the Bragg condition. This phenomenon is referred to as wavelength degeneracy, as depicted in Figure 2B.[27]

The diffractive optical elements using holographic technique have been employed in the AR glasses to direct the projected image to the user's eye to perform see-through function in a compact form factor which is extremely important to practical applications.[5,12,18] However, this device could provide extremely compact form factor to a see-through glasses, the color fidelity is always a problem owing to the dispersion of grating. A quantitative comparison of the color gamut of different diffractive devices is highly demanded. This paper delves into an exploration of the spatial and spectral responses of volume gratings/holograms when utilized in near-eye AR glasses. A noteworthy aspect of this study lies in our novel approach employing holographic multiplexing to enhance the color gamut of VHOE-type AR glasses, and enabling a substantial comparison of color gamut coverage with the SRG approach, all while preserving other essential properties such as the field of view (FOV). As a result, this research offers valuable insights for the development of practical and efficient diffractive light guide systems tailored for near-eye AR glasses applications.

RESULTS AND DISCUSSION

Principle of diffractive light guide

The design of the light guide hinges on the diffraction characteristics of its diffractive elements, as depicted in Figure 3. When SRGs are incorporated into the light guide, the grating dispersion causes the diffraction light to split into various angles, each corresponding to a different wavelength. To ensure optimal performance for a full color display, the diffracted light must propagate at angles in the range limited by the critical angle and glasses configuration, thereby reaching the second SRG with a reflectivity of 100% in principle through TIR. The color-split light is subsequently converged into white light using a second SRG, allowing the projection image to be directed toward the user's eyes. This process is flawless when the diffraction efficiency is ideally 100%. However, since an SRG involves a surface structure, any imperfection in the structure can lead to energy transfer to the leakage mode. This, in turn, may cause the image to diffract in the opposite direction, posing

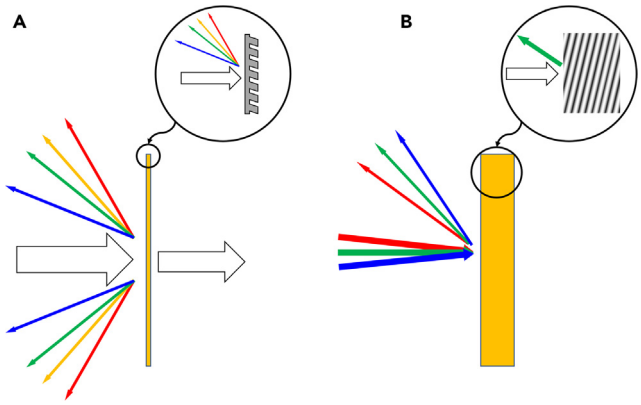

Figure 2. The scenarios of light diffracted from two different gratings
(A) An SRG performs perform dispersion and multi-order of diffraction with white light incidence.
(B) A VHOE performs Bragg condition with high spatial/spectral selectivity. The effective diffraction for a certain wavelength is determined with the incidence condition of the reading light.

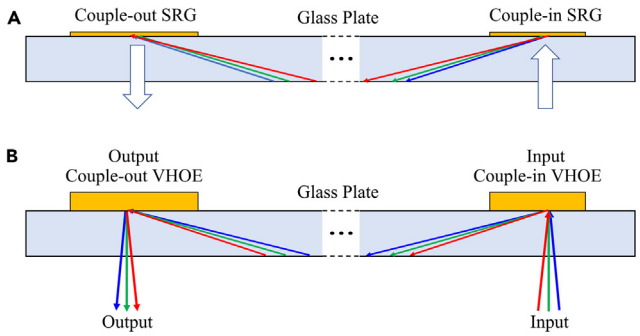

Figure 3. Schematic diagram of the light guide system with two different gratings
(A) SRGs and (B) VHOEs.

potential security or privacy concerns. The second concern is that, due to the dispersion of the grating causing light with three primary colors to propagate at different angles, it is often required to incorporate multiple guide plates with specifically designed gratings for each primary color to enable TIR for all colors, ensuring the maintenance of full-color operation within the designated FOV.[28]

When VHOEs are seamlessly integrated into the light guide, all light with three primary colors can propagate with the same guiding mode within a single guide plate. This is achieved by employing three multiplexed gratings, each based on its own specific Bragg condition. However, the application of the Bragg condition facilitates effective diffraction at diverse angles for different wavelengths.[29,30] In contrast to the conditions in SRG, the second VHOE adeptly steers the color-split light within the light guide toward specific angles, rather than converging it into a unified white image. Consequently, the resultant observed image exhibits a color distribution reminiscent of a rainbow structure. This characteristic introduces a notable challenge to color uniformity, as the perceived wavelength at a given pixel varies laterally from others in the image.

For a comprehensive analysis of the diffraction properties, it is imperative to calculate the diffraction efficiency of both the SRG and the VHOE. In order to facilitate a meaningful comparison, as illustrated in Figure 4, we have standardized key parameters for both the SRGs and the multiplexed gratings of VHOE for three primary colors. These include the horizontal grating periods for red, green, and blue, set at 519.1 nm, 431.5 nm, and 370.7 nm, respectively. The refractive indices for SRG, VHOE, and the glass plate are uniform at 1.505. Additionally, the slanted angle of the grating (ϕ) is fixed at 27.5°, the depth, d of the SRG structure is 200 nm, and the thickness, t of the VHOE is 16 μm.

To further streamline the light guide conditions and prevent crosstalk among the red, green, and blue light, we assume the presence of three distinct light guides for both SRG and VHOE. The RSoft was employed for simulating the diffraction efficiency of the SRG,[31] while Kogelnik's formula was applied to simulate the Bragg diffraction within an FOV of 20°, as depicted in Figure 5.[23] This visualization underscores the fundamental disparity between SRG and VHOE. The former allows all colors to manifest at each viewing angle, albeit with non-uniform diffraction efficiency. In contrast, the latter adheres to the Bragg condition, permitting only a specific bandwidth of red, green, and blue light to be visible at each angle. The distinctive color characteristics of SRG and VHOE exert a discernible influence on the color gamut of the resulting image, elucidating the essential differences between the two optical elements.

Color gamut characteristics

To elucidate the limitations of the two diffractive light guides, we introduced two distinct spectra for the display panel, encompassing red, green, and blue light, as illustrated in Figure 6. These spectra can be generated through either the self-emission of the panel featuring OLED or micro-LED arrays,[32–34] or through panel illumination methods such as Liquid Crystal on Silicon (LCoS) or Digital Light Processing (DLP).[35–37] The first spectrum resembles a laser-like emission with a narrow band, while the second adopts an LED-like emission characterized by Gaussian functions. The color distribution calculations for the light guides employing SRG and VHOE are presented in Figure 7.[38,39] The theoretical modeling and calculation process are presented in the STAR Methods section. Each triangle within the figures signifies the presence of red, green, and blue light in the image at specific viewing angles.

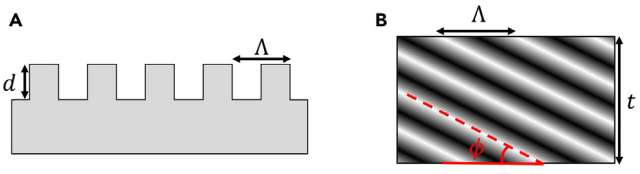

Figure 4. Schematic diagram of two different gratings in the simulation
(A) SRG and (B) VHOE.

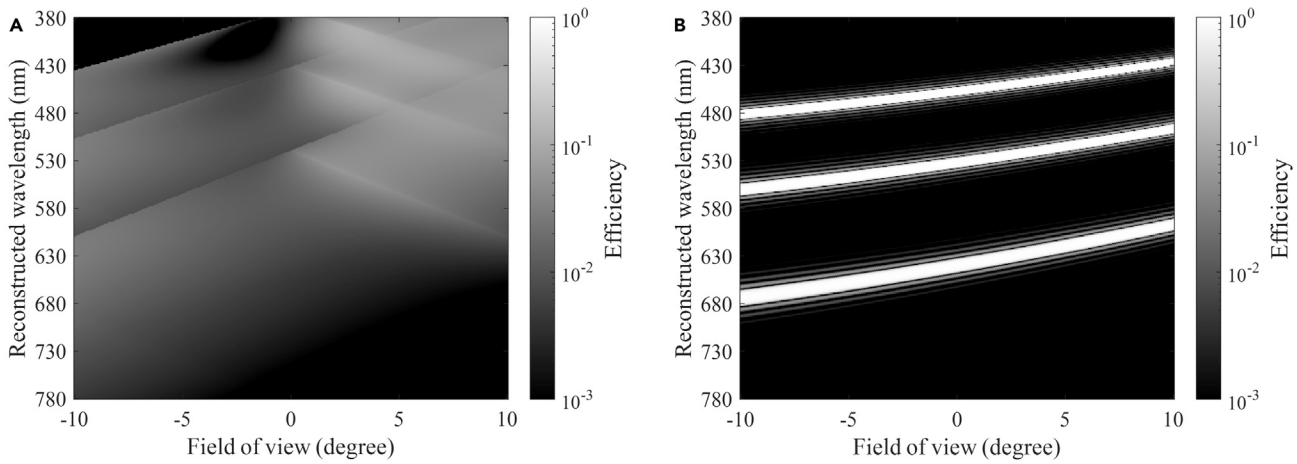

Figure 5. Diffraction efficiency vs. field of view of the image for two different gratings
(A) SRG and (B) VHOE.

In the case of a narrow-band spectrum, the color triangle exhibited by the SRG is identical to that of the VHOE, as illustrated in Figures 7A and 7B. When the spectrum narrows to a laser-like configuration, the image produced by the SRG light guide appears flawless. However, in the VHOE light guide, a complete image is absent, and only fragmented images manifest at three specific viewing angles. This means that the image with narrow-band spectrum will cause the FOV broken. Therefore, the laser-like spectrum is not applicable to a VHOE light guide. It is an important characteristic when VHOEs are used in a see-through light-guide glasses.

For the broad-band spectrum, multiple triangles are evident in both the SRG and VHOE light guides for different viewing angles. In the SRG light guide, as shown in Figure 7C, the overlap area created by these triangles, the common color gamut, is slightly reduced compared to the scenario in Figure 7A, yet remains within an acceptable range. Conversely, the triangles within the VHOE light guide exhibit significant rotation, as shown in Figure 7D, resulting in the common color gamut of the VHOE light guide being insufficient for generating high-quality images. This rotation, induced by the Bragg condition of wavelength degeneracy, constrains the common color gamut to a specific region, even though the image is no longer fragmented within the designated FOV. To mitigate the substantial rotation of the triangles and thereby expand the common color gamut, it is imperative to narrow the bandwidth of red, green, and blue light visible at each viewing angle. To address this challenge, we propose here innovative scheme to multiplex additional volume holograms within the VHOE for providing flexibility to adjust the color coordinates of the primary RGB color at each viewing angle. Holographic multiplexing stands out as a key advantage of the reflective VHOE, where strong coupling strength can yield nearly 100% diffraction efficiency for each multiplexed hologram theoretically.

Our multiplexing scheme is devised to align the peak wavelength of the Gaussian distribution of the light source with the central part of the diffraction efficiency curve of each color, as illustrated in Figure 8A for two sets of volume holograms within the VHOE. This design ensures that the diffracted light is confined near the peak of the Gaussian within a larger viewing angle range, while being equally divided into two parts centered on the peak of the Gaussian within a smaller viewing angle range. As a result, color differences across the entire viewing angle can be minimized, thereby expanding the common color gamut. The conditions of these two sets of volume holograms are as follows. The lateral grating periods for red, green, and blue are 0.519 μm, 0.432 μm, and 0.371 μm, respectively. The corresponding slanted angles are

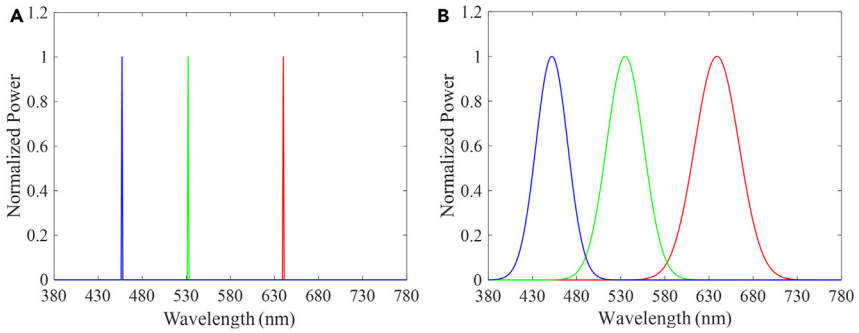

Figure 6. Two different spectra covering red, green and blue light
(A) laser-like spectra in narrow band, (B) broad-band spectra with Gaussian functions.

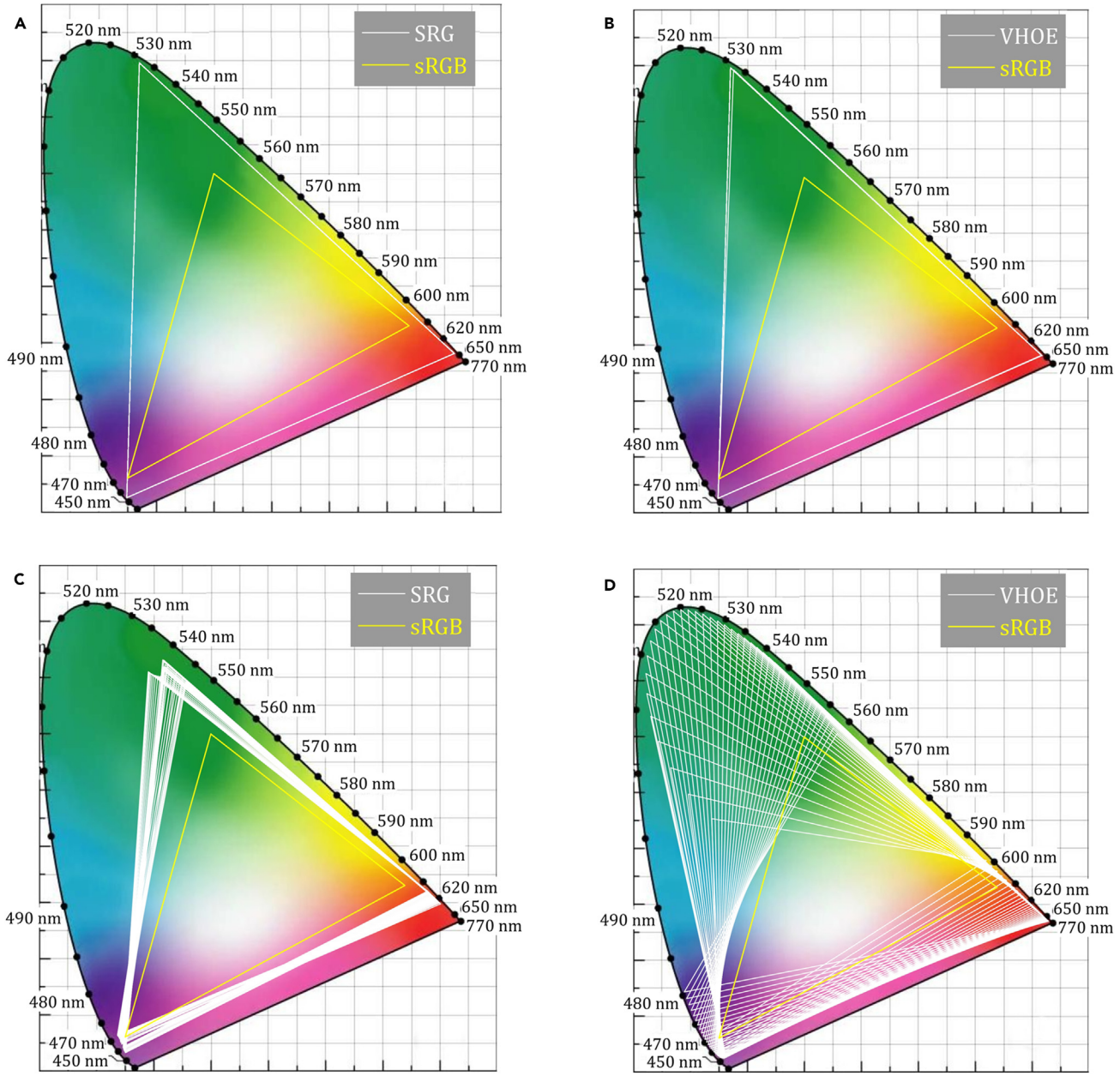

Figure 7. The color gamut distribution of various viewing images

(A) The SRG with light of narrow-band spectrum, (B) the VHOE with light of narrow-band spectrum, (C) the SRG with light of broad-band spectrum, (D) the VHOE with light of broad-band spectrum.

26.13° (red#1), 29.01° (red#2), 26.31° (green#1), 29.42° (green#2), 26.50° (blue#1), and 29.42° (blue#2), respectively. With these conditions, the corresponding color gamut distribution for each viewing angle is depicted in Figure 8B.

While the common color gamut of approximately 130% sRGB in the VHOE light guide may not surpass the 194% sRGB achieved by the SRG light guide with a laser-like spectrum, it closely aligns with the common color gamut of around 133% sRGB when subjected to a broad-band spectrum typical of LED-like emissions from the display panel. Figure 9 provides a comparative analysis of the color gamut versus the FOV of the image for the SRG/VHOE light guide and the standard sRGB. A quantitative comparison of the common color gamut is illustrated in Table 1. Notably, under a broad-band spectrum, the color performance of both the SRG and VHOE light guides exhibits remarkable similarity. Consequently, the color gamut constraint inherent in a VHOE light guide can be alleviated through the meticulous design of holographic multiplexing in VHOEs and the adoption of a suitable broad-band spectrum emitted or reflected from the display panel. This strategic

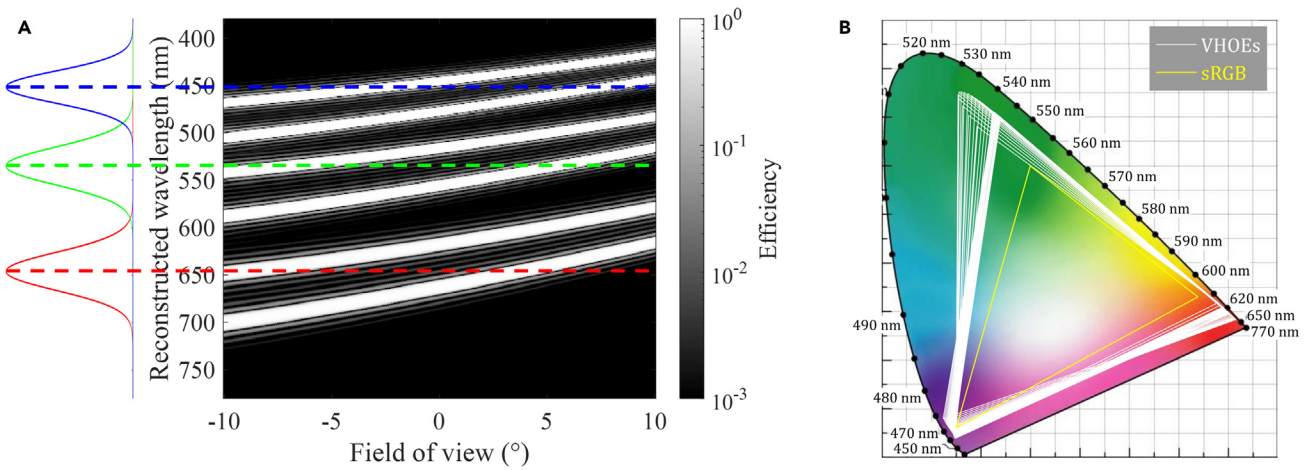

Figure 8. The diffraction efficiency curves of VHOE with multiplexed holograms and corresponding color gamut distribution

(A) The diffraction efficiency vs. the viewing angle for a VHOE with two volume holograms in each primary color. The color lines indicate the peak wavelength of the spectrum.

(B) The corresponding color gamut distribution by each viewing angle.

approach opens avenues for enhancing the color performance of VHOE light guides, bringing them closer to the standards set by broad-band spectrum applications, such as those typical of LED technology.

Conclusions

In this paper, we delve into the distinctive diffraction characteristics of SRG and VHOE deployed in diffractive light guides for near-eye AR glasses. While both act as diffractive reflectors, SRG inherently possesses a thin grating, contrasting with the thick grating nature of VHOE. Notably, the color dispersion in SRGB and wavelength degeneracy in VHOE act different color characteristics.

In the case of SRG, the dispersion effect impacts the requirement for a high refractive index in the glass plate, potentially leading to content security concerns due to leakage modes. On the other hand, VHOE relies heavily on the strict Bragg condition, and its wavelength degeneracy facilitates effective diffraction in a spatial-spectral pair of the input image.

This disparity in color dispersion and degeneracy effects gives rise to distinct color performances. The evaluation of color performance is conducted with three gratings covering red, green, and blue light, respectively. For a laser-like spectrum from the display panel, the color gamut reaches an impressive 194% sRGB. However, this narrow-band spectrum proves challenging for a VHOE light guide, as the diffracted image is viewable only within a limited viewing angle, hindering the complete image visibility.

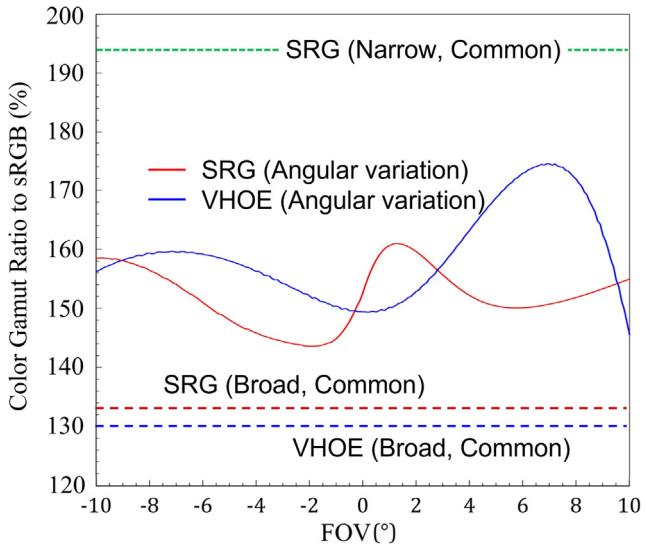

Figure 9. The color gamut ratio to sRGB vs. viewing angle

Here "Common" means the common color gamut for all viewing angles, and means that the color gamut does not vary angularly.

Table 1. A quantitative comparison of color gamut through different approaches

Type of Coupler	SRG	VHOE (W/o Multiplexing)	VHOE (W/- Multiplexing)
Color gamut for narrow bandwidth (Laser-like)	194%	194%	194%
Color gamut for wide bandwidth (LED-like)	133%	50%	130%

In contrast, a broad-band spectrum, such as that produced by an LED, alters the color gamut triangle for an SRG light guide as viewing angles change. The common color gamut decreases to 133% sRGB. Meanwhile, a VHOE light guide experiences erratic rotations of the color gamut triangle, resulting in a common color significantly below the sRGB standard, rendering such a condition unacceptable.

To address this challenge and enhance color performance, we propose a novel multiplexing of two sets of holograms for a VHOE. By aligning the peak wavelength around the middle of the diffraction for the entire FOV, the color gamut triangle undergoes minimal rotation. Our calculations demonstrate that the common color gamut can reach 130% sRGB, nearly matching that achieved by the SRG light guide. This innovation clarifies the color performance of diffractive light guides like SRG and VHOE, rendering them suitable for high-quality near-eye glasses.

STAR★METHODS

Detailed methods are provided in the online version of this paper and include the following:

- KEY RESOURCES TABLE
- RESOURCE AVAILABILITY
  - Lead contact
  - Materials availability
  - Data and code availability
- METHOD DETAILS
  - Calculation of color gamut in a light guide with DOEs
- QUANTIFICATION AND STATISTICAL ANALYSIS

ACKNOWLEDGMENTS

The author would like to thank all team members' efforts in Taiwan MR&3D Team. The research has been sponsored by the National Council for Science and Technology, Taiwan with grant no. MOST 110-2218-E-008-006 -MBK, MOST 111-2218-E-008-004 -MBK, and NSTC 112-2218-E-008-008 -MBK. The authors would also like to express their appreciation for the RSoft software donation from the Synopsys, Inc.

AUTHOR CONTRIBUTIONS

Conceptualization, C.C.S. and S.H.L.; Methodology, W.K.L., W.C.S., and S.K.Z.; Investigation, C.C.S., W.K.L., T.H.Y., W.C.S., and S.K.Z.; Writing – Original Draft, C.C.S.; Writing – Review and Editing, S.H.L., C.S., and Z.F.C.; Funding Acquisition, C.C.S., T.H.Y., and S.H.L.; Supervision, W.C.S., Y.W.Y., T.X.L., and C.Y.C.

DECLARATION OF INTERESTS

The authors declare no competing interests.

Received: January 28, 2024
Revised: April 19, 2024
Accepted: May 15, 2024
Published: May 18, 2024

REFERENCES

1. Kress, B.C. (2020). Optical Architectures for Augmented-, Virtual-, and Mixed-Reality Headsets (SPIE).
2. Zhan, T., Yin, K., Xiong, J., He, Z., and Wu, S.T. (2020). Augmented reality and virtual reality displays: perspectives and challenges. iScience *23*, 101397.
3. Ding, Y., Yang, Q., Li, Y., Yang, Z., Wang, Z., Liang, H., and Wu, S.T. (2023). Waveguide-based augmented reality displays: perspectives and challenges. eLight *3*, 24.
4. Huang, H., and Hua, H. (2018). High-performance integral-imaging-based light field augmented reality display using freeform optics. Opt Express *26*, 17578–17590.
5. Yoshida, T., Tokuyama, K., Takai, Y., Tsukuda, D., Kaneko, T., Suzuki, N., Anzai, T., Yoshikaie, A., Akutsu, K., and Machida, A. (2018). A plastic holographic waveguide combiner for light-weight and highly-transparent augmented reality glasses. J. Soc. Inf. Disp. *26*, 280–286.
6. Yin, K., Lee, Y.H., He, Z., and Wu, S.T. (2019). Stretchable, flexible, and adherable polarization volume grating film for waveguide-based augmented reality displays. J. Soc. Inf. Disp. *27*, 232–237.
7. Anderson, M.J., and Whitcomb, P.J. (2007). DOE Simplified: Practical Tools for Effective Experimentation (Productivity Press).
8. Tamir, T., and Peng, S.T. (1977). Analysis and design of grating couplers. Appl. Phys. *14*, 235–254.
9. Miller, J.M., de Beaucoudrey, N., Chavel, P., Turunen, J., and Cambril, E. (1997). Design and fabrication of binary slanted surface-relief gratings for a planar optical interconnection. Appl. Opt. *36*, 5717–5727.

10. Xu, M., and Hua, H. (2019). Methods of optimizing and evaluating geometrical light guides with microstructure mirrors for augmented reality displays. Opt Express *27*, 5523–5543.
11. Wang, Q., Cheng, D., Hou, Q., Gu, L., and Wang, Y. (2020). Design of an ultra-thin, wide-angle, stray-light-free near-eye display with a dual-layer geometrical waveguide. Opt Express *28*, 35376–35394.
12. Cheng, D., Wang, Q., Wei, L., Wang, X., Zhou, L., Hou, Q., Duan, J., Yang, T., and Wang, Y. (2022). Design method of a wide-angle AR display with a single-layer two-dimensional pupil expansion geometrical waveguide. Appl. Opt. *61*, 5813–5822.
13. Xiong, J., Hsiang, E.L., He, Z., Zhan, T., and Wu, S.T. (2021). Augmented reality and virtual reality displays: emerging technologies and future perspectives. Light Sci. Appl. *10*, 216.
14. Yin, K., He, Z., Xiong, J., Zou, J., Li, K., and Wu, S.T. (2021). Virtual reality and augmented reality displays: advances and future perspectives. J. Phys. Photonics *3*, 022010.
15. Kress, B.C., and Cummings, W.J. (2017). 11-1: invited paper: towards the ultimate mixed reality experience: HoloLens display architecture choices. Symp. Digest Tech. Pap. *48*, 127–131.
16. Devagiri, J.S., Paheding, S., Niyaz, Q., Yang, X., and Smith, S. (2022). Augmented Reality and Artificial Intelligence in industry: Trends, tools, and future challenges. Expert Syst. Appl. *207*, 118002.
17. Zhang, Y., and Fang, F. (2019). Development of planar diffractive waveguides in optical see-through head-mounted displays. Precis. Eng. *60*, 482–496.
18. Nakamura, T., and Takashima, Y. (2018). Design of discretely depth-varying holographic grating for image guide based see-through and near-to-eye displays. Opt Express *26*, 26520–26533.
19. Waldern, J.D., Grant, A.J., and Popovich, M.M. (2018). DigiLens switchable Bragg grating waveguide optics for augmented reality applications. Proc. SPIE. Digit. Opt. Immersive Disp. *10676*, 108–123.
20. Gu, Y., Weng, Y., Wei, R., Shen, Z., Wang, C., Zhang, L., and Zhang, Y. (2022). Holographic waveguide display with large field of view and high light efficiency based on polarized volume holographic grating. IEEE Photon. J. *14*, 1–7.
21. Yin, K., Lee, Y.H., He, Z., and Wu, S.T. (2019). Stretchable, flexible, rollable, and adherable polarization volume grating film. Opt Express *27*, 5814–5823.
22. Lee, Y.H., Yin, K., and Wu, S.T. (2017). Reflective polarization volume gratings for high efficiency waveguide-coupling augmented reality displays. Opt Express *25*, 27008–27014.
23. He, L., Chen, X., Yang, Y., Liu, X., Chen, Y., Xu, L., and Gu, C. (2023). Using high-diffraction-efficiency holographic optical elements in a full-color augmented reality display system. Opt Express *31*, 29843–29858.
24. Kogelnik, H. (1969). Coupled wave theory for thick hologram gratings. Bell Syst. Tech. J. *48*, 2909–2947.
25. Yariv, A., and Yeh, P. (1984). Optical Waves in Crystals: Propagation and Control of Laser Radiation (Wiley).
26. Goodman, J.W. (2002). Introduction to Fourier Optics (McGraw-Hill).
27. Liu, W., Barbastathis, G., and Psaltis, D. (2004). Volume holographic hyperspectral imaging. Appl. Opt. *43*, 3581–3599.
28. Mukawa, H., Akutsu, K., Matsumura, I., Nakano, S., Yoshida, T., Kuwahara, M., and Aiki, K. (2009). A full-color eyewear display using planar waveguides with reflection volume holograms. J. Soc. Inf. Disp. *17*, 185–193.
29. Sun, C.C., and Banerjee, P.P. (2004). Volume holographic optical elements. Opt. Eng. *43*. https://doi.org/10.1117/1.1790505.
30. Sun, C.C. (2003). Simplified model for diffraction analysis of volume holograms. Opt. Eng. *42*, 1184–1185.
31. Moharam, M.G., and Gaylord, T.K. (1981). Rigorous coupled-wave analysis of planar-grating diffraction. J. Opt. Soc. Am. *71*, 811–818.
32. Huang, Y., Hsiang, E.L., Deng, M.Y., and Wu, S.T. (2020). Mini-LED, Micro-LED and OLED displays: present status and future perspectives. Light Sci. Appl. *9*, 105.
33. Wu, T., Sher, C.W., Lin, Y., Lee, C.F., Liang, S., Lu, Y., Huang Chen, S.-W., Guo, W., Kuo, H.-C., and Chen, Z. (2018). Mini-LED and micro-LED: promising candidates for the next generation display technology. Appl. Sci. *8*, 1557.
34. Park, J., Choi, J.H., Kong, K., Han, J.H., Park, J.H., Kim, N., Lee, E., Kim, D., Kim, J., Chung, D., et al. (2021). Electrically driven mid-submicrometre pixelation of InGaN micro-light-emitting diode displays for augmented-reality glasses. Nat. Photonics *15*, 449–455.
35. Huang, Y., Liao, E., Chen, R., and Wu, S.T. (2018). Liquid-crystal-on-silicon for augmented reality displays. Appl. Sci. *8*, 2366.
36. Krum, D.M., Suma, E.A., and Bolas, M. (2012). Augmented reality using personal projection and retroreflection. Personal Ubiquitous Comput. *16*, 17–26.
37. Yin, K., Hsiang, E.L., Zou, J., Li, Y., Yang, Z., Yang, Q., Lai, P.C., Lin, C.L., and Wu, S.T. (2022). Advanced liquid crystal devices for augmented reality and virtual reality displays: principles and applications. Light Sci. Appl. *11*, 161.
38. International Electrotechnical Commission (1999). IEC 61966-2-1: 1999 Multimedia Systems and Equipment– Colour Measurement and Management– Part 2-1: Colour Management– Default RGB Colour Space– sRGB.
39. CIE (2004). CIE 15: 2004-Colorimetry (CIE).

STAR★METHODS

KEY RESOURCES TABLE

REAGENT or RESOURCE	SOURCE	IDENTIFIER
Software and algorithms		
MATLAB	MATLAB Software Foundation	https://www.matlab.org
RSoft	Synopsys, Inc.	https://www.synopsys.com
POWERPOINT	Microsoft Corporation	https://www.microsoft.com
GRAPHER	Golden Software	https://www.goldensoftware.com

RESOURCE AVAILABILITY

Lead contact

Any additional information required to reanalyze the data reported in this work paper is available from the lead contact upon request, Shiuan Huei Lin (lin@nycu.edu.tw).

Materials availability

This study did not generate new unique reagents.

Data and code availability

- All data reported in this paper will be shared by the lead contact upon request.
- This paper does not report original code.
- Any additional information required to reanalyze the data reported in this paper is available from the lead contact upon request.

METHOD DETAILS

Calculation of color gamut in a light guide with DOEs

Our Augmented Reality (AR) eyewear display, illustrated in below figure for the model of a diffractive light-guide system, is primarily composed of two diffractive gratings, a guide plate, and a light engine with an illumination spectra of three primary RGB colors shown as Figure 7B. Here, we should note that in our setup, the micro-display in light engine is located at the front focal plane of a projected lens. The light from each pixel can be converted into a plane wave with a wave-vector, k_i (as shown in the inserted plot in below figure), reaching to the couple-in DOE with incident wavelength and angles of (λ,θ,ϕ). The angle (θ,ϕ) can then be considered as the corresponding viewing angle of each pixel from the micro-display in our case. To calculate the color gamut perceived by the human eye for each viewing angle, the color tri-stimulus for three primary colors must be calculated firstly. In order to accomplish this, we modify the formula of the tri-stimulus values by integrating the diffraction efficiency of the diffractive grating,[39] and it can be written as,

$$X_i(\theta,\phi) = \int S_i(\lambda)\eta^2(\lambda,\theta,\phi)\overline{x}(\lambda)d\lambda$$

$$Y_i(\theta,\phi) = \int S_i(\lambda)\eta^2(\lambda,\theta,\phi)\overline{y}(\lambda)d\lambda \qquad \text{(Equation 1)}$$

$$Z_i(\theta,\phi) = \int S_i(\lambda)\eta^2(\lambda,\theta,\phi)\overline{z}(\lambda)d\lambda$$

where the S_i is spectra of each primary color denoted as $i = r, g, b$; η is diffraction efficiency of diffractive grating; (θ,ϕ) is the incident angle of plane wave corresponding to each pixel; and $\overline{x}(\lambda),\overline{y}(\lambda),\overline{z}(\lambda)$ present CIE 1931 2° standard observers for current AR glasses characteristic. The RSoft is employed for simulating the diffraction efficiency of the SRG so that the color tri-stimulus can be obtained numerically. In contrast, for VHOE, the equation, derived from coupled wave theory,[24,25] reveals the diffraction efficiency varies with incident angles and wavelength can be written as,

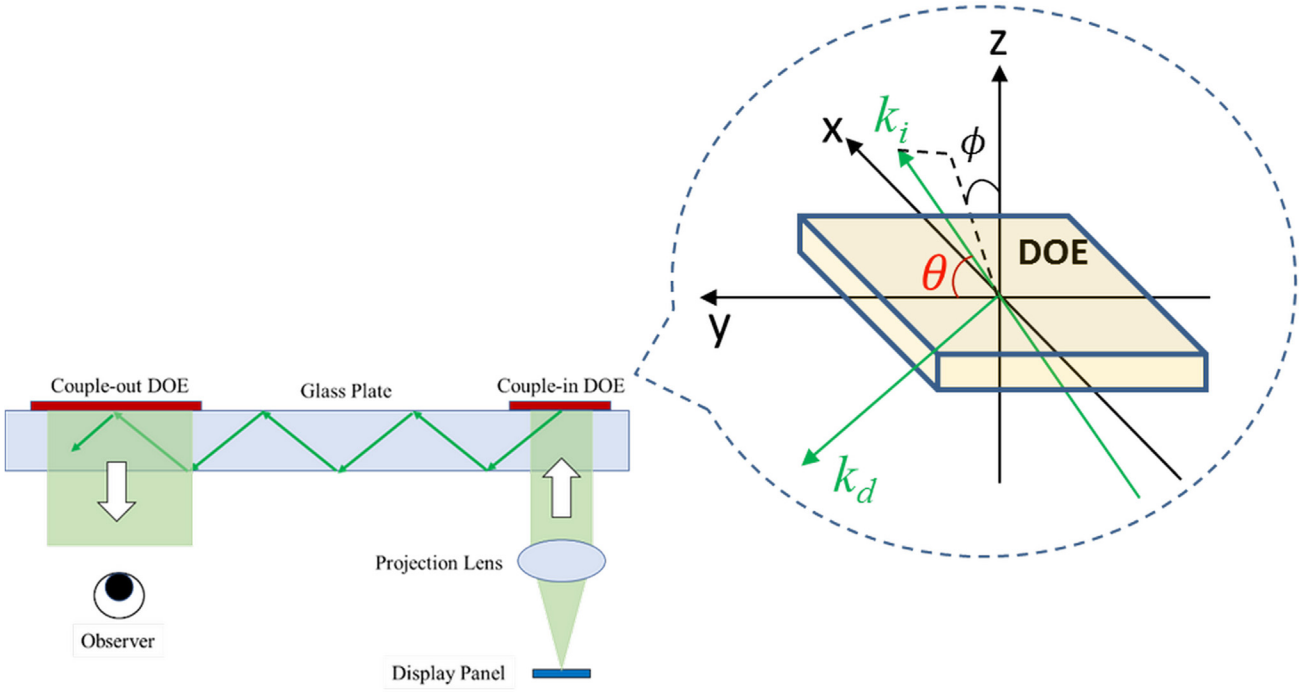

Schematic diagram of a diffractive light-guide system for AR eyewear display

$$\eta(\lambda,\theta,\phi) = \frac{|\kappa_{12}\kappa_{21}| * sinh^2(A' * d)}{\left(\frac{\Delta\beta}{2}\right)^2 * sinh^2(A' * d) + A'^2 * cosh^2(A' * d)} \quad \text{(Equation 2)}$$

where A' is given by

$$A' = \sqrt{\kappa_{12}\kappa_{21} - \left(\frac{\Delta\beta}{2}\right)^2} \quad \text{(Equation 3)}$$

We note κ_{12} *and* κ_{21} are coupling constants with the depth of index modulation, Δn and the plane wave from pixel on micro-display with the incident angle of (θ,ϕ) and the corresponding diffracted angle of (θ_d,ϕ_d) after the coupling DOE. They are given by

$$\kappa_{12} = \frac{\pi * \Delta n}{\lambda} * \frac{1}{\sin(\theta)\cos(\phi)}; \quad \kappa_{21} = \frac{-\pi * \Delta n}{\lambda} * \frac{1}{\sin(\theta_d)\cos(\phi_d)} \quad \text{(Equation 4)}$$

and a momentum mismatch

$$\Delta\beta = \beta_d - \beta_i - K_z \quad \text{(Equation 5)}$$

where β_d, β_i, K_z are wave-vector components along the z-axis of the incident light, the diffracted light and the coupling VHOE grating. They are given by

$$\beta_i = \frac{2\pi}{\lambda} n_0 * \sin(\theta)\cos(\phi), \beta_d = \frac{2\pi}{\lambda} n_0 * \sin(\theta_d)\cos(\phi_d),$$

$$K_z = \frac{2\pi}{\lambda_g} n_0 * [\sin(\theta_2')\cos(\phi_2') - \sin(\theta_1')\cos(\phi_1')] \quad \text{(Equation 6)}$$

where n_0 is the averaged index of refraction of the medium of the VHOE. λ_g, (θ_1', ϕ_1') and (θ_2', ϕ_2') are the wavelength of light, incident angles of the reference and signal waves, respectively during the recording of VHOEs. Thus, the color tri-stimulus for three primary colors can be calculated as all the parameters are given according to the AR glasses system. The CIE 1931 *x-y* chromaticity coordinates of three primary colors can then be obtained by the definitions,

$$(x_i, y_i) = \left(\frac{X_i}{X_i+Y_i+Z_i}, \frac{Y_i}{X_i+Y_i+Z_i}\right) \quad \text{(Equation 7)}$$

where $i = r, g, b$ is noted for each primary color. They are noted on the CIE chart for indicating the color gamut for different pixel on the micro-display. With the parameters shown in Figure 5, we can obtain and show the color gamut of the incident light from the pixels with the corresponding incident angles of $\theta = 0, \pm 5°$ and $\phi = 0$ as examples for both SRG and VHOE cases, shown in below figure. Following the same steps, we can obtain all the color gamut shown in Figures 7 and 8 for the detail discussions in the main text.

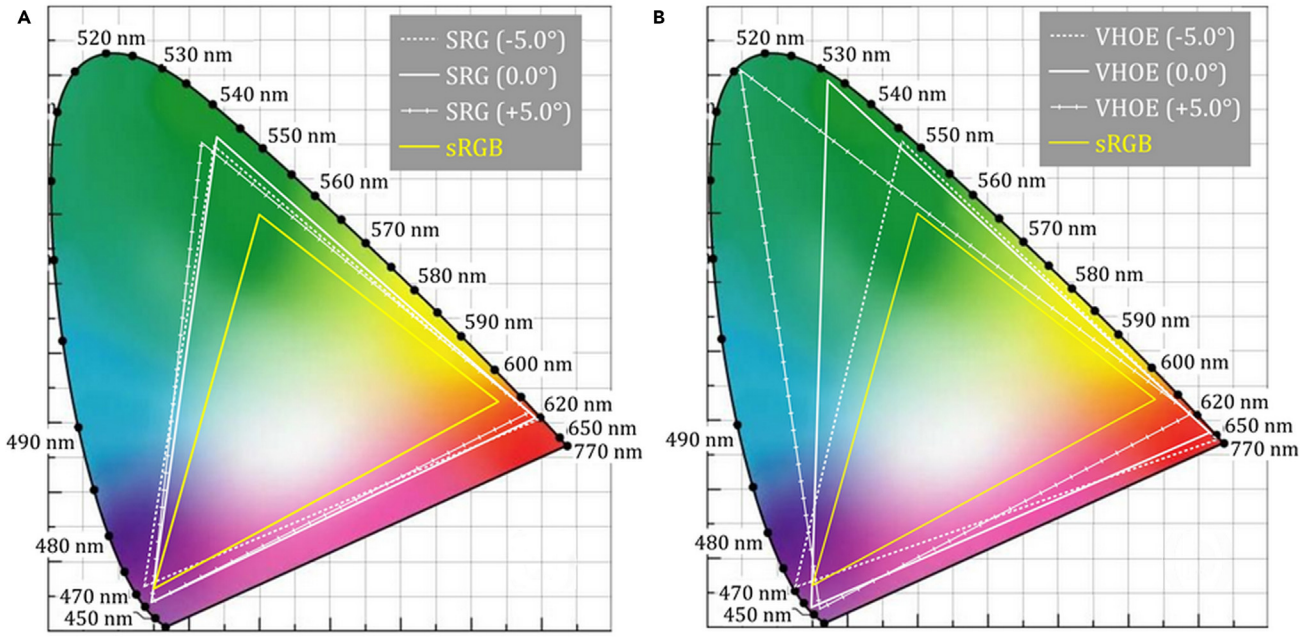

The color gamut of the viewing image, $\theta = 0, \pm 5°, \varphi = 0$
(A) the SRG, (B) the VHOE.

QUANTIFICATION AND STATISTICAL ANALYSIS

In this work, through theoretical derivation, we obtain the Equations 1, 2, 3, 4, 5, 6, and 7 in the section of method details. According to the system parameters, we make numerical simulation by MATLAB software. Using the simulation data produced by MATLAB software, Figures 5, 7, and 8 shown in the main text were produced by GRAPHER from the raw data. Moreover, the diagrammatic Figures 1, 2, and 3 as well as figure in the calculation of color gamut in a light guide with DOEs section are drawn by POWERPOINT software.